npj | quantum information

Article

Published in partnership with The University of New South Wales

https://doi.org/10.1038/s41534-024-00816-x

Efficient bosonic nonlinear phase gates

Kimin Park [1] ✉ & Radim Filip [1]

Continuous-variable (CV) quantum information processing harnesses versatile experimental tools that leverage the power of infinite-dimensional oscillators controlled by a single qubit. Increasingly available elementary Rabi gates have been proposed as a resource for implementing universal CV gates, but the requirement of many weak, non-commuting gates is a bottleneck in scaling up such an approach. In this study, we propose a resource-efficient technique using Fourier expansion to implement arbitrary non-linear phase gates in a single oscillator. This method reduces the number of sequentially required gates exponentially. These gates represented by cubic, quartic, and other arbitrary nonlinear potentials have applications in CV quantum information processing with infinite-dimensional oscillators controlled by a single qubit. Our method outperforms previous approaches and enables the experimental realization of a wide range of applications, including the development of bosonic quantum sensors, simulations, and computation using trapped ions and superconducting circuits.

Continuous-variable (CV) quantum information processing using infinite-dimensional oscillators[1–5] offers a promising alternative to the more commonly used discrete-variable (DV) approach based on photons[6–8] or other particles[9–11]. It is particularly advantageous when the DV approach requires a large number of qubits to simulate the CV effects. However, to fully harness the power of CV systems for quantum computation, it is essential to efficiently implement arbitrary nonlinear operations on them. This principal requirement can be mainly achieved by a bridge—the third order (cubic)[12–16] and, subsequently, higher-order non-linearities derived due to nontrivial commutation relations. While this approach is effective, it can be made more efficient by directly accessing higher-order nonlinearities and multi-system gates, as in DV systems.

A hybrid Rabi gate beyond the rotating wave approximation serves as a key resource empowering various CV approaches for full non-linear control. These gates involve deep-strong couplings between a CV oscillator and a DV two-level system[17,18]. They are widely available in various experiments involving trapped ions[9,19–24] and superconducting circuits[25–29] among many others, and can be implemented effectively by coherent Hamiltonian control in photonic and molecular crystal systems[30–38] where the bosonic mode is represented by a microwave, a phononic, or even an optical field. Moreover, the incremental approach[39] based on these gates can achieve universality in CV quantum computation. It can also be efficiently simulated with the aid of a parametric process[40]. However, the current incremental approaches for accurately implementing nonlinear phase gates require a large number of weak, non-commuting Rabi gates, presenting a significant constraint due to the effects of decoherence and the accumulation of precision errors from implementations. Recently, an approach to harness the power of non-commutative Fourier transforms to enable precise manipulation and control of time-dependent dynamics of complex quantum systems within an extended Floquet framework was proposed[41].

In this work, we introduce a highly efficient method for directly engineering strong non-linear CV phase gates. Our approach uses a finite-order Fourier expansion, demonstrating an exponential enhancement in resource efficiency compared to previous methods. By optimizing the non-commuting qubit Pauli matrices in the Rabi gates to reproduce the coefficients of the Fourier expansion, we can efficiently perform nonlinear transformations on CV systems with minimal resource usage. This technique can significantly advance CV quantum information processing and bridge the gap in experimental capability for universal CV computation[39,42]. This is crucial since highly accurate nonlinear gates [14] are necessary for such computation to take place.

Rabi gates, described by the generators $\hat{H}_j^{\Theta} = \hat{\sigma}_j \hat{X}_{\Theta}$ where $j = \mathrm{x}, \mathrm{y}, \mathrm{z}$, can be interconverted through simple rotations in the qubit or oscillator. Qubit Pauli operators $\hat{\sigma}_j$ do not commute with each other and satisfy the commutation relation $[\hat{\sigma}_j, \hat{\sigma}_k] = 2\mathrm{i}\epsilon_{jkl}\hat{\sigma}_l$ with the Levi-Civita symbol ϵ_{jkl}. The angles of the oscillator quadrature operators $\hat{X}_{\Theta} = \frac{\hat{a}\mathrm{e}^{-\mathrm{i}\Theta} + \hat{a}^{\dagger}\mathrm{e}^{\mathrm{i}\Theta}}{\sqrt{2}}$ are commonly set to $\Theta = 0, \pi/2$, resulting in the abbreviations $\hat{X} \equiv \hat{X}_0$ and $\hat{P} \equiv \hat{X}_{\frac{\pi}{2}}$, referred to as X-Rabi and P-Rabi gates respectively. This work focuses on methods based *solely* on X-Rabi gates that contain variable qubit Pauli operators, which simplify the implementations and improve stability across a wide range of input states.

[1]Department of Optics, Palacky University, 77146 Olomouc, Czech Republic.
✉e-mail: park@optics.upol.cz

The previous method constructs phase gates $\hat{U}(\hat{X}_k) \equiv \exp(i\chi_k \hat{X}_k)$ with a specific order of non-linearity k and strength χ_k among arbitrary unitary gates on the oscillator $\hat{U}(V(\hat{X})) \equiv \exp(i\chi_V(\hat{X}))$. This is achieved using an adjoint form of X-Rabi gates with non-commutative Pauli matrices only at right angles[39,42]. This incremental approach alone has been demonstrated to supply the universal CV gate set in a proof-of-principle manner, but its feasibility for implementation is limited due to the requirement for rapid control of many pulses to achieve strong nonlinear gates through a high number of repetitions.

Results

Finite series expansion of CV gates

This work approximates the target phase gates $\hat{U}(\hat{X}^k)$ through a finite N-th order Fourier series expansion. The resulting general superposition of displacements is given by:

$$\hat{U}(\hat{X}^k) \approx \exp[i\gamma\hat{X}] \sum_{l=-N/2}^{N/2} C_l \exp[i l t_f \hat{X}], \quad (1)$$

where an auxiliary displacement provided deterministically by a Rabi gate with amplitude γ may be applied to increase the accuracy of the approximation. The complex coefficient C_l is calculated using a Fourier series expansion as $C_l = |\frac{t_f}{2\pi}| \int_{-\pi/t_f}^{\pi/t_f} dx \exp[i\chi_k x^k] \exp[-i l t_f x]$. The optimal values for C_l, N, and the Fourier component interval t_f are determined to maximize the fidelity (defined in Supplementary Section I) with the ideal states, or any alternative figure of merit. Advantageously, the expansion based on the Fourier series is guaranteed to saturate the target function $\hat{U}(V(\hat{X}))$ asymptotically with a large N, requiring fewer pulses than a previous method to achieve the desired accuracy.

To achieve efficient and deterministic implementation of nonlinear phase gates, we can use the non-commuting qubit Pauli matrices in the Rabi gates to reproduce coefficients C_l in a finite-order Fourier expansion of Eq. (1) for superposed displacement gates. Figure 1a describes the basic concept and the target gates. Advantageously, this method avoids the need for sequential measurement and re-preparation of the qubit, and instead uses Pauli operations to control non-commuting Rabi gates in the qubit part. To implement the target gate $\hat{U}(\hat{X}^k)$, N Rabi gates with a fixed strength t are applied in a sequence:

$$\hat{O} \equiv \exp[i\gamma\hat{X}] \prod_{j=1}^{N} \exp[i t \hat{\sigma}_{\theta_1^{(j)},\theta_2^{(j)}} \hat{X}]. \quad (2)$$

These X-Rabi gates have a Pauli matrix $\hat{\sigma}_{\theta_1,\theta_2} \equiv \cos\theta_1 \hat{\sigma}_z + \sin\theta_1 \cos\theta_2 \hat{\sigma}_x + \sin\theta_1 \sin\theta_2 \hat{\sigma}_y$ containing variable angles $\theta_{1,2}$, and the overlap between the eigenstates of the individual jth Pauli matrices $\hat{\sigma}_{\theta_1^{(j)},\theta_2^{(j)}}$ controls C_l to achieve the target gate.

For the specific case of simulating a cubic gate $\hat{U}(\hat{X}^3)$ being the main testing case of this paper for a comparison with the previous works[39,42], the Fourier coefficients C_l are real due to the sign parity. Therefore, the cubic gate simulation only needs non-zero angles of θ_1, and the other angles are unnecessary as $\theta_2 = 0$ in the Pauli matrix. This can be expressed equivalently as the Rabi gates together with the qubit rotations as $\exp[it\hat{\sigma}_{\theta_1,0}\hat{X}] = \exp[-i\frac{\theta_1}{2}\hat{\sigma}_y] \exp[it\hat{\sigma}_z\hat{X}] \exp[i\frac{\theta_1}{2}\hat{\sigma}_y]$. The $\hat{\sigma}_z$ in Rabi gate can be replaced with $\hat{\sigma}_x$ equivalently in ideal situations, while this substitution may make the protocol more vulnerable to qubit dephasing that happens during the Rabi gates. The qubit eigenstates of such a Rabi operator

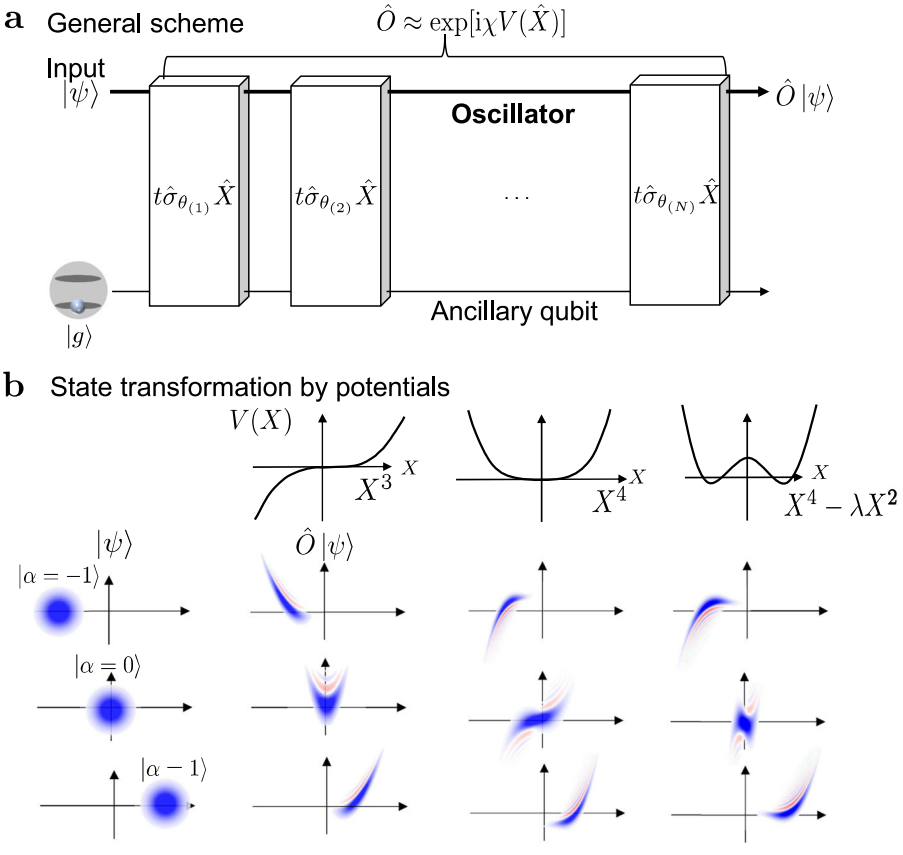

Fig. 1 | Efficient implementation of nonlinear phase gates using Rabi gates with variable qubit angles. a Conceptual diagram of the Fourier method. The Fourier expansion of an ideal nonlinear gates $\hat{U}(V(\hat{X})) = \exp[i\chi V(\hat{X})]$ can be implemented by using a few tens of Rabi gates with variable qubit angles and auxiliary oscillator displacements to accurately transform chosen input states. Each Rabi gate is fine-tuned by fast, coherent changes to the qubit state by Pauli rotations. The qubit is traced out after the sequence of tuned Rabi gates, resulting in a mixed state on the oscillator. Alternatively, the gate can be simulated slightly more accurately by post-selecting specific qubit measurement outcomes, at the minor cost of success probability. **b** Examples of state transformation by various target phase gates engineered by the proposed Fourier method. The illustrations show the simulation of non-linear potentials on coherent states $|\alpha\rangle$, including cubic, quartic, and double-well potentials, but the scheme is not limited to these. Coherent states along the momentum axis in the form $|\alpha = \pm i|\alpha|\rangle$ have the same performance and the shapes of Wigner function as vacuum input states, except for the location, and can therefore be represented using the example of the vacuum state input. The Wigner functions of the states after ideal gates are indistinguishable from the results of the Fourier methods. Overall, this approach allows for an accurate implementation of nonlinear phase gates using a minimal number of Rabi gates with variable qubit angles.

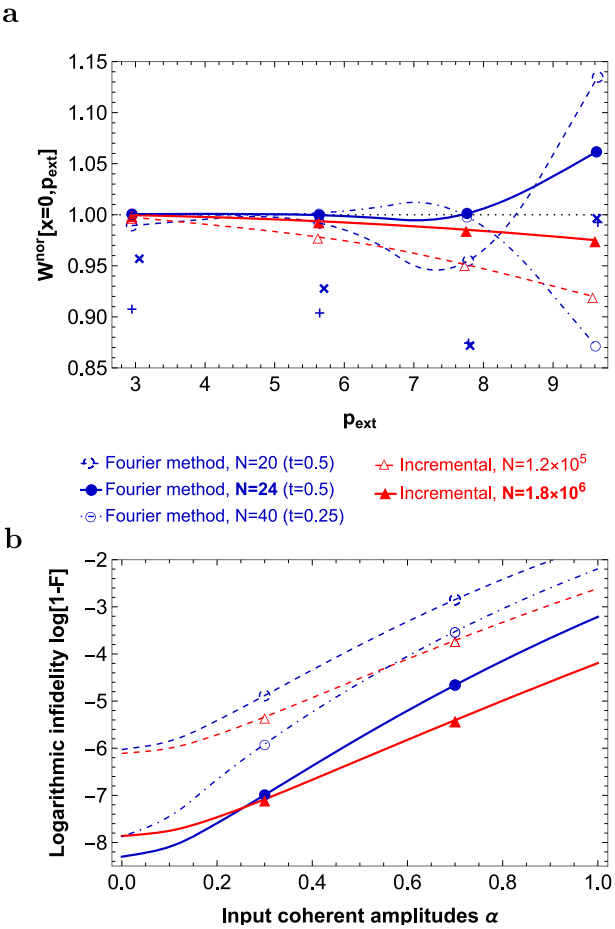

Fig. 2 | Comparison of the Fourier Method and Incremental Method Performance. a Comparison of normalized negative peaks of Wigner functions against the ideal peaks as defined in (4) for the cubic phase gate of $\chi_3 = 1.0$ generated by different methods acting on the vacuum state. We used the Fourier method based on an optimal finite series expansion with $N = 20$ and 24 Rabi gates of Rabi strength 0.5, corresponding to a total Rabi cost of $tN = 10$ and $tN = 12$, respectively. A faster qubit control but with the same total resource with $N = 40$ and $t = 0.25$ is also compared. Total dephasing of $q_{tot} = 0.2$ (Marked by "+") and bosonic loss $\eta_{tot} = 0.04$ ("×") were applied to test the stability. A reference line 1 for the ideal gate is displayed for comparison, and guidelines are provided to aid in peak identification. Our findings reveal that the Fourier method reproduces ideal peaks with greater accuracy and resource efficiency compared to the incremental method. However, the Fourier method's finite approximation results in some instability in the simulation of the small fourth negative peak. **b** Logarithmic in-fidelity vs. coherent amplitudes of coherent states $|\alpha\rangle$. Markers of the curves serves only for identification, while 10 data points were used for all curves. Our results indicate that the Fourier method's fidelity is comparable to the incremental method, which requires a larger amount of resources for the cases tested. As the total number of Rabi gates N increases, the fidelity using Fourier method approaches negative infinity more quickly. However, states far from the origin may have larger errors due to the finite approximation. **b** No noise or loss was included for illustrative purposes. The expected fidelity drop to the gate number can be modelled as $F_{N,p} \approx F_{N,0}(1-p)^N$ for a low per-gate infidelity $p << 1$.

are given as $|+_{\theta_1}\rangle = \exp[-i\frac{\theta_1}{2}\hat{\sigma}_y]|e\rangle$ and $|-_{\theta_1}\rangle = \exp[-i\frac{\theta_1}{2}\hat{\sigma}_y]|g\rangle$, where $|e\rangle$, $|g\rangle$ are the eigenstates of $\hat{\sigma}_z$. The overlaps of these eigenstates of different Pauli operators are summarized as

$$\langle s'_{\theta'_1}|s_{\theta_1}\rangle \equiv \cos\left[\phi + (s'-s)\frac{\pi}{4}\right] \tag{3}$$

for $s, s' = \pm 1$ and $\phi = \frac{\theta_1 - \theta'_1}{2}$. These angles θ_1 and θ'_1 can be controlled experimentally to simulate the target gate faithfully. The key difference between our protocol and the incremental method[39] is that the latter uses Rabi gates with Pauli matrices fixed along σ_x, σ_y, and σ_z having eigenstates that form right angles of $\pi/2$ on the Bloch sphere. In contrast, our method allows the angles of the Pauli matrices, or the relative qubit rotation angles between Rabi gates, to take on continuous values that can be optimized. These arbitrary, continuously tunable angles are central to achieving the enhanced efficiency and fidelity of our Fourier approach. Determining the optimal angle settings is at the core of our method, and we describe the numerical optimization to maximize fidelity in more detail in the Supplementary Material.

Under the constraints regarding the normalization of the states, we can sequentially construct a wide range of approximate operations $\hat{O}$ with $|C_l| \leq 1$ (Supplementary Material III). These operations are sufficient for simulating the unitary phase gates of interest. When the angles are appropriately chosen, the implemented functions converge quickly to the target gates with minimal resource usage. We can optimize the fidelity of the gates applied to the vacuum state to find the optimal control parameters for the Rabi gates, particularly the overlap in (3). While the individual jth Rabi strength $t^{(j)}$ can also be adjusted for better performance, this requires greater computational resources for numerical optimization and greater experimental control. For the sake of simplicity, a fixed t is used in this manuscript. The superiority of this method, as demonstrated in the subsequent analysis, arises from the fact that no inverse Rabi operation is required to cancel out lower-order terms, as is necessary for the incremental approach. Consequently, this method is exceptionally resource-efficient, allowing for the implementation of powerful gates with minimal resource usage.

Stability analysis

The stability of the Fourier method for experimental realizations is analyzed by examining major imperfections in both the auxiliary qubit and oscillator system. In trapped ions, the auxiliary qubit is typically assumed to be lossless and not subject to amplitude damping, but still sensitive to small phase damping[9,10]. The different case typical for the superconducting circuits[25–29] is discussed in the Supplementary Material. The qubit dephasing occurs during individual Rabi gates, which are the key resource of the scheme. The qubit phase damping is modeled using the channel $\Gamma_q[\rho] = (1-\frac{q}{2})\rho + \frac{q}{2}\hat{\sigma}_z\rho\hat{\sigma}_z$ for any state ρ, where the dephasing parameter $q = 1 - e^{-\gamma_q t}$ ranges from 0 (no dephasing) to 1 (maximum dephasing). For a cavity QED implementation, we also consider bosonic loss in the optical mode as another potential threat to the scheme. Any density matrix ρ undergoing bosonic loss channel Γ_η evolves as $\Gamma_\eta[\rho] = \sum_{l=0}^{\infty}\frac{(1-\eta)^l}{l!}\eta^{\hat{n}/2}\hat{a}^l\rho\hat{a}^{\dagger l}\eta^{\hat{n}/2}$, where the loss parameter is defined as $\eta = e^{-\gamma t} \in (0,1]$ and γt is the dimensionless damping parameter, equivalent to Kraus operator notation in ref. 43. This is equivalent to the solution of the Lindblad equation $\partial_t\rho = \hat{L}\rho\hat{L}^\dagger - \frac{1}{2}\{\hat{L}^\dagger\hat{L}\rho\}$ with Lindblad operator with $\hat{L} = \sqrt{\gamma}\hat{a}$. We can model qubit relaxation through spontaneous emission using the Lindblad master equation with Lindblad operator $\hat{\sigma}_-$. This noise source is present in systems like trapped ions and superconducting qubits, although usually less significant than dephasing or photon loss. The solution of the Lindblad equation for an arbitrary initial qubit state can be characterized by a single parameter $r = \exp(-\gamma t_{\text{relax}}/2)$, where γt_{relax} represents the dimensionless qubit loss. The effect of qubit amplitude damping on the system's density matrix ρ is: $\rho = c_{gg}|g\rangle\langle g| + c_{ee}r^2|e\rangle\langle e| + c_{ee}(1-r^2)|g\rangle\langle g| + rc_{eg}|e\rangle\langle g| + rc_{ge}|g\rangle\langle e|$ where c_{ij} are the input density matrix elements. This compactly encapsulates the dissipative dynamics from qubit relaxation. At each Rabi gate, a constant level of dephasing (dq), boson loss ($d\eta$), and qubit loss dr is applied for simplicity of analysis, while they may depend on the Rabi strength t as longer Rabi gate times allow more accumulation of errors proportional to the gate duration. The total dephasing parameter and the total loss parameter scales roughly as $q_{tot} \approx N(dq)$, $r_{tot} \approx (dr)^N$ and $\eta_{tot} \approx (d\eta)^N$. Increasing resource usage, such as the Rabi strength and number of gates, can overcome low noise levels due to the improved approximation but provides diminishing returns at very high noise. A brief summary of the result is given in the Supplementary Material.

The presence of negative values in the Wigner function serves as a signature of quantum non-Gaussian behavior, and their accurate

reproduction verifies that the core quantum interference aspect is simulated effectively. It is observed at the lowest resource usage for the input ground state among all coherent states in the oscillator, as shown in Fig. 1b. The phase-space interference for other input coherent states is complex, so we primarily focus on evaluating the interference for the input ground state.

In Fig. 2a, we compared the Wigner functions of the output states ρ from the intial vacuum state $|0\rangle$ (e.g., a simulated state $\rho^{\text{sim}} = \hat{O}|0\rangle\langle 0|\hat{O}^\dagger$ and imperfect states $\Gamma_q[\rho^{\text{sim}}]$ and $\Gamma_\eta[\rho^{\text{sim}}]$) at the negative peaks normalized against those of the ideal cubic state $\rho^{\text{ideal}} = \hat{U}|0\rangle\langle 0|\hat{U}^\dagger$, defined as

$$W^{\text{nor}}[x=0, p_{\text{ext}}^{(j)}[\rho]] = \frac{W[x=0, p_{\text{ext}}^{(j)}[\rho]; \rho]}{W[x=0, p_{\text{ext}}^{(j)}[\rho^{\text{ideal}}]; \rho^{\text{ideal}}]} \tag{4}$$

where $p_{\text{ext}}^{(j)}[\rho]$ denotes the location of p-quadrature of the jth negative local minimum of the Wigner function of the density matrix ρ. The normalized negative peaks are used to measure the accuracy of the approximation. A ratio 1 indicates a perfectly reproduced peak, and a different value represents an error in the approximation. The accuracy of the peak locations also confirms the reliability of the simulation. We investigate the first 4 negative peaks of $j = 1, 2, 3, 4$. The resource usage is quantified by the total Rabi strength used in the simulation (tN for the Fourier method), and the number of total Rabi gates (N for the Fourier method), as these quantities are directly related to the total decoherence effects. Generally, increasing both the total Rabi cost tN and the total number of gates N improves the simulation.

Our analysis of the normalized negative Wigner peaks demonstrates that the Fourier expansion method is more resource-efficient in approximating the essential quantum properties of the ideal phase gates than the incremental method. In particular, the Fourier method reproduces the primary negative peaks of Wigner functions with high accuracy, even when compared to the incremental method, which requires a greater amount of resources. To verify the stability of the new method, we considered a qubit dephasing and boson loss per Rabi gate in the 20 Rabi gates protocol. Our findings indicate that all the negative peaks are stable under such conditions. Even when subjected to high levels of total dephasing of $= 0.2$ and bosonic loss $\eta_{tot} = 0.04$, the first two negative peaks retain over 90% of the ideal depths. However, we found that the finite approximation of the Fourier method may cause the smaller negative peaks of Wigner functions to exceed the ideal peaks, resulting in an overshooting effect. Nevertheless, the presence of dephasing and loss can partially mitigate this effect.

In Fig. 2b, we compare the Fourier method to the incremental method in terms of logarithmic infidelity. It is defined as $\log[1 - F]$ where F is the fidelity between the target state and the approximate state. Using 20 Rabi gates with fixed strength $t = 0.5$ (total Rabi strength of $tN = 10.0$), the Fourier method achieves a fidelity 0.998 to the target ideal cubic gate with strength $\chi_3 = 1$ for coherent states with purely imaginary amplitudes $|\alpha = \pm i|\alpha|\rangle$ with $|\alpha| \in [-\infty, \infty]$ including vacuum state, and the fidelity for input coherent state with real amplitudes $|\alpha = \pm 0.5\rangle$ drops slightly to 0.978. To benchmark the gate's performance more comprehensively, we evaluate the fidelity of thermal states in addition to coherent states. Thermal states represent the infinite entropy mixture of all states within a given photon number constraint. The fidelity for thermal states at mean photon number exceeds the fidelity for coherent states, for example at $\bar{n} = 0.25$ when it was given as 0.985. This demonstrates our gate functions well for superpositions of photon number states, complementing the coherent state analysis. Evaluating performance on both coherent and thermal states provides a robust characterization. In comparison, the incremental method requires a huge resource of approximately $N = 1.2 \times 10^5$ Rabi gates and total Rabi strength of $tN = 10^4$ to achieve a similar fidelity. The Fourier method can be improved rapidly by using a slightly more resource. For example, the Fourier method with $N = 24$ Rabi gates (with total Rabi strength $tN = 12$) performs similarly to an incremental method using approximately $N = 1.8 \times 10^6$ Rabi gates and total Rabi strength of $tN = 10^5$ to give a similar fidelity of $\log[1 - F] \approx -8$. The in-fidelity scaling by the Fourier method can be approximately described as $\log[1 - F] \approx -0.65 - 0.31N$ for $t = 0.5$ around $N \in [20, 40]$. In contrast, the incremental method shows the in-fidelity scaling described as $\log[1 - F] \approx 1.59 - 0.66 \log N$ around $N \in [10^5, 3 \times 10^6]$. The exponential fidelity scaling demonstrates that the Fourier method provides an exponential improvement in resource efficiency compared to the incremental method.

To comprehensively benchmark the gate, we evaluated performance using more stringent metrics beyond fidelity. Specifically, we analyzed the trace distance $D[\rho_1, \rho_2] = \text{tr}|\rho_1 - \rho_2|/2$ between the ideal and actual gate outputs, which quantifies state distinguishability. Trace distance D ranges from 0 to 1, with 0 meaning the states are identical. The trace distance also followed logarithmic and linear scaling with gate number N for the incremental and Fourier methods, respectively, given as $\log D \approx 4.01 - 0.66 \log N$ and $\log D \approx -0.07 - 0.16N$. This efficient scaling further verifies the exponential enhancement in resource efficiency with the Fourier method.

Moreover, we can enhance the accuracy of the approximation further by keeping the total Rabi strength constant and increasing only the number of total Rabi gates. For instance, the Fourier method with $N = 40$ Rabi gates with total Rabi strength $tN = 10.0$ achieves a much higher fidelity of 0.9996, much higher than that with $N = 20$ and the same total Rabi strength. This improvement in fidelity is consistent across coherent states. In the asymptotic limit of fast gate control where $N \to \infty$ and $tN \to \infty$, the fidelity approaches 1 for all α, and the approximate gate becomes the ideal gate more rapidly than the incremental methods.

The advantage of the Fourier method becomes more apparent in the presence of realistic effects, due to the complexity of the protocol of the incremental methods. Our observations indicate that the Fourier method achieves robustness >500 times higher than the incremental method under the same levels of noise. Moreover, this advantage in robustness can be improved even further by optimization of the strengths of the Rabi gates.

Extension to the quartic gate and beyond

The implementation of quartic gates or other nonlinear potentials using the Fourier expansion requires complex Fourier coefficients. These complex coefficients can be obtained by using Pauli matrices $\hat{\sigma}_{\theta_1^{(j)}, \theta_2^{(j)}}$ with non-zero qubit rotation angles $\theta_{1,2}$ in (2), which can be implemented using general qubit rotations between Rabi gates. Our findings demonstrate that the Fourier approach can achieve a fidelity 0.9988 (0.9932) for a quartic gate with $\chi_4 = 0.2$ using $N = 20$ (10) Rabi gates with a total Rabi strength $tN = 10$ (5). In contrast, achieving this level of fidelity using the incremental method would require a large number of Rabi gate, for example, a total Rabi strength of about $tN = 40000$ (321), with approximately $N = 0.5 \times 10^6$ (2400) Rabi gates for a fidelity of 0.9988 (0.9932). This highlights that the Fourier approach can provide an approximately 4000-fold and 24000-fold (60-fold and 240-fold) enhancement in terms of total Rabi strength and total number of Rabi gates for this quartic gate with different fidelity levels. Again, an exponential enhancement in resource scaling is observed. The negative Wigner functions for the ideal quartic gates and simulated ones by the Fourier method are also very close, as shown in the Supplementary Material.

The quintic gate $\exp[i\chi_5 \hat{X}^5]$ and higher odd-ordered phase gates can be efficiently simulated near the phase-space origin using the Fourier method with X-Rabi and a single type of qubit rotation, similar to the cubic gate. However, even-ordered phase gates require two types of qubit rotations, similar to the quartic gate. The parity of the target phase gate, therefore, affects the efficiency and stability of the protocol. Similar to the quartic gate, the Fourier method can simulate a double-well potential of the form $\exp[i\chi_4 \hat{X}^4 + i\chi_2 \hat{X}^2]$ with comparable performance to that of the quartic gate, as demonstrated in Supplementary Material.

Discussion

This work confronts critical aspects of challenges in efficiently implementing arbitrary nonlinear operations on CV systems. The holistic approximation via the Fourier series differs from the previous incremental Trotterization method that constructs each phase gate individually based on the Baker-Campbell-Hausdorff theorem and then recombines them. The Fourier expansion approach provides a new pathway for compiling

arbitrary nonlinear gates, broadening the applicability of CV quantum information processing. It bridges the gap between digital and analog gate synthesis techniques, marking a conceptual blending of methods. In summary, the Fourier method opens up a wide range of applications and experimental opportunities in ref. 19 trapped ions[9,20–24] and superconducting circuits[25–29]. These opportunities include the development of bosonic quantum sensors, as well as simulation and computation.

Our proposed Fourier approach for efficient nonlinear bosonic gates could be implemented in several leading experimental platforms[44], including trapped ion systems and superconducting circuits. Trapped ions offer long coherence times and exquisite control over both the motional and spin degrees of freedom, making them well-suited for realizing the variable-angle Rabi gates required for the Fourier technique[9,10,19–22,24,43]. However, scaling trapped ion systems to large numbers of qubits and achieving faster gate times remain ongoing challenges. Superconducting circuits provide a complementary platform, where strong couplings between microwave cavities and transmon qubits enable fast, high-fidelity entangling gates[25–29]. While coherence times are steadily improving, reducing the gate time below ~100 ns and achieving higher fidelities will be key hurdles. Integrated photonic circuits could be another intriguing candidate, where electro-optic modulation can produce the variable Rabi couplings between light and matter[45,46]. Current challenges include achieving sufficiently strong nonlinearities in CMOS-compatible devices. In all cases, improving qubit coherence, faster and higher-power modulators for the Rabi gates, and fast high-fidelity control and measurement would significantly advance the prospects for implementing the Fourier approach across these platforms. While technical challenges remain, our proposed technique brings universal CV gates closer to reality on multiple leading quantum computing platforms.

Alternative gate sets exist that could potentially simulate CV operations efficiently, such as using selective photon number (SNAP) gates combined with displacements[47,48]. SNAP gates allow selective rotations of quantum states within a chosen Fock subspace, providing a powerful tool for state engineering primarily in superconducting circuits. The Fourier approach provides a distinct and direct way to engineer nonlinear bosonic gates, without assuming prior knowledge of the input state. In particular, SNAP gates inherently rely on an incremental approach to implement rotations between Fock states $|n\rangle$ and $|n+1\rangle$. Constructing strong gates that require large rotation, analogous to cubic or higher-order nonlinear phase gates, would require many repetitions of SNAP and displacement gates, limiting resource efficiency. The strong nonlinear gates needed for CV operations involve large off-diagonal matrix elements in the Fock basis, making them challenging to efficiently simulate with SNAP techniques. In contrast, both the target cubic gates and the Rabi gates used in the Fourier technique are diagonal in the position basis, enabling more direct and efficient engineering. While SNAP gates present other advantages like robustness and high efficiency in other types of operation like Kerr gates, the Fourier method provides an alternative approach to realizing nonlinear bosonic operations. Exploring combinations of these techniques may unlock further benefits. Overall, having multiple available routes to implementing universal CV gates will ultimately aid efficient simulation. We note that the Fourier approach outlined in this study can be directly adapted for implementing higher-order Kerr gates utilizing dispersive gates.

Data availability

The numerical data presented in this study is available from the authors upon request.

Code availability

All codes will be available on request.

Received: 20 March 2023; Accepted: 2 February 2024;
Published online: 23 February 2024

References

1. Braunstein, S. L. & Loock, P. V. Quantum information with continuous variables. *Rev. Mod. Phys.* **77**, 513 (2005).
2. Cerf, N. J., Leuchs, G. & Polzik, E. S. (eds) Quantum information with continuous variables of atoms and light (World Scientific (World Scientific, New Jersey, 2007).
3. Weedbrook, C. et al. Gaussian quantum information. *Rev. Mod. Phys.* **84**, 621 (2012).
4. Andersen, U. L., Neergaard-Nielsen, J. S., Van Loock, P. & Furusawa, A. Hybrid discrete-and continuous-variable quantum information. *Nat. Phys.* **11**, 713–719 (2015).
5. Lvovsky, A. I. et al. Production and applications of non-gaussian quantum states of light. https://arxiv.org/abs/2006.16985 (2020)
6. Kok, P. et al. Linear optical quantum computing with photonic qubits. *Rev. Mod. Phys.* **79**, 135 (2007).
7. O'brien, J. L., Furusawa, A. & Vuckovic, J. Photonic quantum technologies. *Nat. Photonics* **3**, 687–695 (2009).
8. Flamini, F., Spagnolo, N. & Sciarrino, F. Photonic quantum information processing: a review. *Rep. Prog. Phys.* **13**, 016001 (2018).
9. Bruzewicz, C. D., Chiaverini, J., McConnell, R. & Sage, J. M. Trapped-ion quantum computing: progress and challenges. *Appl. Phys. Rev.* **6**, 021314 (2019).
10. Kjaergaard, M. et al. Superconducting qubits: current state of play. *Annu. Rev. Condens. Matter Phys.* **11**, 369–395 (2020).
11. Vandersypen, L. M. K. & Eriksson, M. A. Quantum computing with semiconductor spins. *Phys. Today* **72**, 38 (2019).
12. Lloyd, S. & Braunstein, S. L. Quantum computation over continuous variables. *Phys. Rev. Lett.* **82**, 1784–1787 (1999).
13. Bartlett, S. D., Sanders, B. C., Braunstein, S. L. & Nemoto, K. Efficient classical simulation of continuous variable quantum information processes. *Phys. Rev. Lett.* **88**, 4 (2002).
14. Budinger, N., Furusawa, A. & van Loock, P. All-optical quantum computing using cubic phase gates. http://arxiv.org/abs/2211.09060 (2022).
15. Marek, P. et al. General implementation of arbitrary nonlinear quadrature phase gates. *Phys. Rev. A* **97**, 1–6 (2018).
16. Hillmann, T. et al. Universal gate set for continuous-variable quantum computation with microwave circuits. *Phys. Rev. Lett.* **125**, 160501 (2020).
17. Forn-Díaz, P., Lamata, L., Rico, E., Kono, J. & Solano, E. Ultrastrong coupling regimes of light-matter interaction. *Rev. Mod. Phys.* **91**, 25005 (2019).
18. Frisk Kockum, A. et al. Ultrastrong coupling between light and matter. *Nat. Rev. Phys.* **1**, 19–40 (2019).
19. Leibfried, D., Blatt, R., Monroe, C. & Wineland, D. Quantum dynamics of single trapped ions. *Rev. Mod. Phys.* **75**, 281 (2003).
20. Kienzler, D. et al. Observation of quantum interference between separated mechanical oscillator wave packets. *Phys. Rev. Lett.* **116**, 140402 (2016).
21. Fluhmann, C. et al. Encoding a qubit in a trapped-ion mechanical oscillator. *Nature* **566**, 513 (2019).
22. Hacker, B. et al. Deterministic creation of entangled atom-light Schrödinger-cat states. *Nat. Photonics* **13**, 110–115 (2019).
23. Brown, K. R., Chiaverini, J., Sage, J. M. & Häffner, H. Materials challenges for trapped-ion quantum computers. *Nat. Rev. Mater.* **6**, 892–905 (2021).
24. Schupp, J. et al. Interface between trapped-ion qubits and traveling photons with close-to-optimal efficiency. *PRX Quantum* **2**, 020331 (2021).
25. Touzard, S. et al. Gated conditional displacement readout of superconducting qubits. *Phys. Rev. Lett.* **122**, 080502 (2019).
26. Campagne-Ibarcq, P. et al. Quantum error correction of a qubit encoded in grid states of an oscillator. *Nature* **584**, 368 (2020).

27. Kwon, S., Tomonaga, A., Lakshmi Bhai, G., Devitt, S. J. & Tsai, J. S. Gate-based superconducting quantum computing. *J. Appl. Phys.* **129**, 041102 (2021).
28. Ma, W. L. et al. Quantum control of bosonic modes with superconducting circuits. *Sci. Bull.* **66**, 1789–1805 (2021).
29. García Ripoll, J. J. Quantum information and quantum optics with superconducting circuits (Cambridge University Press, 2022).
30. Mueller, N. S. et al. Deep strong light-matter coupling in plasmonic nanoparticle crystals. *Nature* **583**, 780–784 (2020).
31. Flühmann, C., Negnevitsky, V., Marinelli, M. & Home, J. P. Sequential modular position and momentum measurements of a trapped ion mechanical oscillator. *Phys. Rev. X* **8**, 021001 (2018).
32. Langford, N. et al. Experimentally simulating the dynamics of quantum light and matter at deep-strong coupling. *Nat. Commun.* **8**, 1715 (2017).
33. Lv, D. et al. Quantum simulation of the quantum rabi model in a trapped ion. *Phys. Rev. X* **8**, 021027 (2018).
34. Braumüller, J. et al. Analog quantum simulation of the Rabi model in the ultra-strong coupling regime. *Nat. Commun.* **8**, 779 (2017).
35. Ballester, D., Romero, G., García-Ripoll, J. J., Deppe, F. & Solano, E. Quantum simulation of the ultrastrong-coupling dynamics in circuit quantum electrodynamics. *Phys. Rev. X* **2**, 021007 (2012).
36. Stassi, R., Cirio, M. & Nori, F. Scalable quantum computer with superconducting circuits in the ultrastrong coupling regime. *npj Quantum Inf.* **6**, 67 (2020).
37. J. Koch, G. Hunanyan,T. Ockenfels,E. Rico,E. Solano,M. W. Quantum Rabi dynamics of trapped atoms far in the deep strong coupling regime. *Nat. Commun.* **14**, 954 (2023).
38. Shitara, T. et al. Nonclassicality of open circuit QED systems in the deep-strong coupling regime. *New J. Physics* https://arxiv.org/abs/2006.16769 (2021).
39. Park, K., Marek, P. & Filip, R. Deterministic nonlinear phase gates induced by a single qubit. *N. J. Phys.* **20**, 053022 (2018).
40. Chen, Y. H., Qin, W., Wang, X., Miranowicz, A. & Nori, F. Shortcuts to adiabaticity for the quantum Rabi model: efficient generation of giant entangled cat states via parametric amplification. *Phys. Rev. Lett.* **126**, 023602 (2021).
41. Guo, L. & Peano, V. Engineering arbitrary hamiltonians in phase space. *Phys. Rev. Lett.* **132**, 023602 (2024).
42. McConnell, P., Ferraro, A. & Puebla, R. Multi-squeezed state generation and universal bosonic control via a driven quantum Rabi model. http://arxiv.org/abs/2209.07958 (2022).
43. Albert, V. V. et al. Performance and structure of single-mode bosonic codes. *Phys. Rev. A* **97**, 032346 (2018).
44. Awschalom, D. D. et al. Development of quantum interconnects (quics) for next-generation information technologies. *PRX Quantum* **2**, 017002 (2021).
45. Wang, J., Sciarrino, F., Laing, A. & Thompson, M. G. Integrated photonic quantum technologies. *Nat. Photonics* **14**, 273–284 (2020).
46. Elshaari, A. W., Pernice, W., Srinivasan, K., Benson, O. & Zwiller, V. Hybrid integrated quantum photonic circuits. *Nat. Photonics* **14**, 285–298 (2020).
47. Kudra, M. et al. Robust preparation of wigner-negative states with optimized snap-displacement sequences. *PRX Quantum* https://arxiv.org/abs/2111.07965 (2022).
48. Fösel, T., Krastanov, S., Marquardt, F. & Jiang, L. Efficient cavity control with snap gates. http://arXiv.org/abs/2004.14256 (2020).

Acknowledgements

R.F. and K.P. acknowledge project 21-13265X of the Czech Science Foundation. We also acknowledge EU H2020-WIDESPREAD-2020-5 Project NONGAUSS (951737) under the CSA-Coordination and Support Action.

Author contributions

All authors designed the protocol. K.P. performed the calculations and simulations. R.F. performed analysis of the results and supervised the work. All authors discussed and interpreted the results, and contributed to the writing of the manuscript.

Competing interests

The authors declare no competing interest.

Additional information

Supplementary information The online version contains supplementary material available at https://doi.org/10.1038/s41534-024-00816-x.

Correspondence and requests for materials should be addressed to Kimin Park.